THE JOURNAL OF PHYSICAL CHEMISTRY C

Article

pubs.acs.org/JPCC

Initial Steps of Thermal Decomposition of Dihydroxylammonium 5,5′-bistetrazole-1,1′-diolate Crystals from Quantum Mechanics

Qi An,‡ Wei-Guang Liu,‡ William. A. Goddard, III,* Tao Cheng, Sergey V. Zybin, and Hai Xiao

Materials and Process Simulation Center, California Institute of Technology, Pasadena, California 91125, United States

Supporting Information

ABSTRACT: Dihydroxylammonium 5,5′-bistetrazole-1,1′-diolate (TKX-50) is a recently synthesized energetic material (EM) with most promising performance, including high energy content, high density, low sensitivity, and low toxicity. TKX-50 forms an ionic crystal in which the unit cell contains two bistetrazole dianions {c-((NO)N_3C)-[c-(CN_3(NO)], formal charge of −2} and four hydroxylammonium $(NH_3OH)^+$ cations (formal charge of +1). We report here quantum mechanics (QM)-based reaction studies to determine the atomistic reaction mechanisms for the initial decompositions of this system. First we carried out molecular dynamics simulations on the periodic TKX-50 crystal using forces from density functional based tight binding calculations (DFTB-MD), which finds that the chemistry is initiated by proton transfer from the cation to the dianion. Continuous heating of this periodic system leads eventually to dissociation of the protonated or diprotonated bistetrazole to release N_2 and N_2O. To refine the mechanisms observed in the periodic DFTB-MD, we carried out finite cluster quantum mechanics studies (B3LYP) for the unimolecular decomposition of the bistetrazole. We find that for the bistetrazole dianion, the reaction barrier for release of N_2 is 45.1 kcal/mol, while release of N_2O is 72.2 kcal/mol. However, transferring one proton to the bistetrazole dianion decreases the reaction barriers to 37.2 kcal/mol for N_2 release and 59.5 kcal/mol for N_2O release. Thus, we predict that the initial decompositions in TKX-50 lead to N_2 release, which in turn provides the energy to drive further decompositions. On the basis of this mechanism, we suggest changes to make the system less sensitive while retaining the large energy release. This may help improve the synthesis strategy of developing high nitrogen explosives with further improved performance.

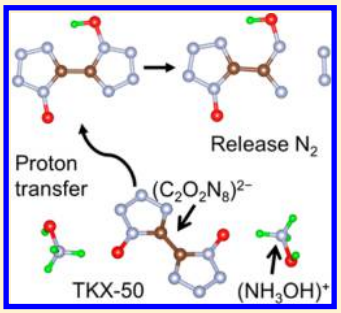

1. INTRODUCTION

Energetic materials (EM) such as pentaerythritol tetranitrate (PETN), 2,4,6-trinitro-toluene (TNT), 1,3,5-trinitro-1,3,5-triazinane (RDX), and 1,3,5,7-tetranitro-1,3,5,7-tetrazocane (HMX) are in extensive use for such civilian applications as mining, building, fire extinguishing systems, and military applications because of fast energy release during decomposition, deflagration, and detonation.[1,2] However, EM with increased energy content are needed that have decreased sensitivity toward external stimuli of heating, friction, and impact.[3] Many efforts are ongoing to design and synthesize new explosives with improved performance.[4−7] Particularly promising candidacies among the new EMs are nitrogen-rich heterocycles (with several nitrogen atoms linked together into a ring) which lead to superior energy release compared to traditional EMs.

The recently synthesized dihydroxylammonium 5,5′-bistetrazole-1,1′-diolate (TKX-50) is an azole-based high energy density material (HEDM) with promising performance because of high exothermicity, high density, and insensitivity toward external stimuli.[8] In addition, it is relatively easy to synthesize with components of low toxicity, making it a promising candidate for a new generation of green EMs. Figure 1 shows the crystal structure of TKX-50 (P_{21}/c space group), with a unit cell consisting of two bistetrazole anions (formal charge of −2) and four hydroxylammonium $(NH_3OH)^+$ cations (formal charge of +1). Although many properties have been studied,[8] the decomposition reaction mechanism of TKX-50 remains

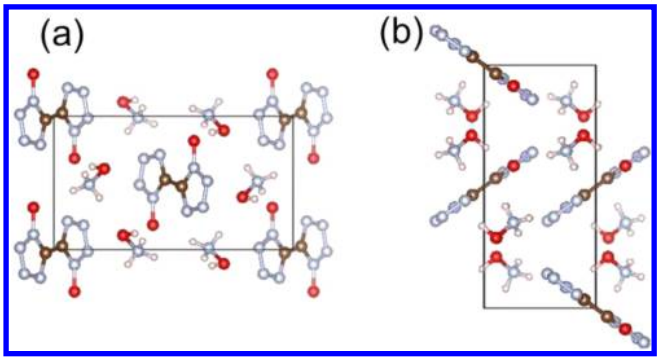

Figure 1. Crystal structure of dihydroxylammonium 5,5′-bistetrazole-1,1′-diolate (TKX-50).[8] The unit cell contains four hydroxylammonium $(NH_3OH)^+$ and two diolate $(C_2O_2N_8)^{2-}$ moieties. The C, H, O, N are represented by brown, white, red, and gray balls, respectively. Panel (a) is the view from the *a* direction, and panel (b) is the view from the *c* direction.

Received: September 22, 2014
Revised: October 27, 2014
Published: October 28, 2014

   dx.doi.org/10.1021/jp509582x | J. Phys. Chem. C 2014, 118, 27175−27181

unknown. In this paper we use quantum mechanics (QM) to predict the initial decomposition steps of TKX-50.

Controlling thermal decomposition of EMs during its storage and transportation is essential because initiating thermal decomposition presents a risk of huge energy release. Thus, it is important to understand the mechanisms of ignition, combustion, and sensitivity due to thermal fluctuations. This provides information useful for designing new EMs with improved stability.[9−12] Uncovering the complex chemical processes underlying initiation of decomposition is essential to build theoretical models to describe the combustion and detonation of TKX-50 and related azole-based HEDMs. Such studies also provide information for synthesizing and designing new energetic materials with improved performance.

The decomposition reaction mechanisms of many EMs have been examined using theoretical[13−21] and experimental methods.[11,12,22−26] For such nitro-based explosives as RDX and HMX, the initial reaction paths involve NO_2 dissociation or HONO elimination.[15,16] In addition, intermolecular hydrogen transfer reaction is observed in such reactions as molten TNT and nitrobenzene.[17,18] Moreover, for the colossally sensitive silapentaerythritol tetranitrate (Si-PETN), a novel carbon−oxygen rearrangement, was found to be induced by a transient five-coordinate Si.[19,20] The initial chemical reactions might be affected by electronic excitation[13] and crystal morphology.[14] Experiments and density functional theory (DFT) calculations[22,23] also suggested that the conformational change of PETN under static and shock compression may play an important role in shock initiation.

To examine the chemical reactions of TKX-50 in the condensed phase, we carried out molecular dynamics simulations on the crystal using forces from periodic quantum mechanics (DFT tight binding, DFTB) to discover the initial reaction steps at high temperature. Then we used finite cluster quantum mechanics (B3LYP) to determine the reactions pathways, transition state geometries, and reaction barriers.

2. METHODOLOGY

2.1. DFTB Molecular Dynamics Simulation. To perform DFTB-MD simulations, we used the self-consistent charge density-functional tight binding (SCC-DFTB) method.[27] The SCC-DFTB method is based on a second-order expansion of the Kohn−Sham total energy in DFT with respect to charge density fluctuations. In order to accurately describe the long-range Coulomb interactions, the general tight binding method is extended using a self-consistent redistribution of Mulliken charges (SCC). These methods have been used to examine the chemical reactions of nitromethane and hydrazoic acid under high temperature and high pressures.[28−30] Our simulations were carried out using the DFTB+ 1.2.2[31] software with the 3ob-2-1 parameter set to describe the interactions of the C−H−O−N system.[32] The accuracy criteria for the charge calculation is 1×10^{-5} e (maximum difference in any charge between two SCC cycles). The Lennard−Jones dispersion model was employed to correct the long-range dispersion interactions; with parameters from the universal force field (UFF).[33] We used a $2 \times 1 \times 2$ periodic supercell that contains 8 anion and 16 cation molecules. Only the gamma point was sampled in the Brillouin zone.

We started with the experimental structure[8] and minimized it using conjugate gradients method. The optimized cell parameters at 0 K from DFTB are a = 5.413 Å, b = 11.586 Å, c = 6.625 Å, and β = 95.40°, compared with the X-ray values of a = 5.487 Å, b = 11.547 Å, c = 6.483 Å, and β = 95.402° at 100 K.[8] Thus, the predicted cell parameters from DFTB (0 K) agree well with the values from experiment (100 K). Since the changes in experimental cell parameters[8] between 100 and 298 K are within 1.8%, we expect the corrections from 100 to 0 K to be small. The maximum deviation of bond lengths, bond angles, and torsion angles are 0.045 Å, 2.1°, and 1.3°, respectively. Then we carried out DFTB-MD at 300 K using the NVT ensemble (constant temperature, constant volume, and constant number of atoms) for 500 fs (time step of 0.25 fs) to equilibrate the structure. Finally we carried out DFTB-MD temperature-programmed cook-off simulations with the temperature increasing continuously from 300 to 3000 K at a heating rate of 180 K/ps (total run time 15 ps).

To be practical, these QM-based cook-off simulations use quite high heating rates, which might lead to unphysical reactions. To examine the reactions at a reduced temperature, we carried out a second simulation starting from the configuration at room temperature. Then we increased it to 1750 K very fast (within 0.5 ps) and carried out a NVT simulation at a fixed temperature of 1750 K for 20 ps. Here we used the Berendsen thermostat (40 fs damping constant) in MD simulations, and the temperature for the electron filling was always set to the simulation temperature.

To analyze the fragments in the DFTB-MD simulations, we determined the atomic connectivity using bond distance cutoffs with a time window of 0.25 ps to avoid miscounting short-term fluctuations in the bonds above the cutoff but which do not actually break (or form) a bond. These bond distance cutoffs are listed in the Table S1 of Supporting Information (SI).

2.2. Finite Cluster QM Calculation. To examine the reaction mechanism in more detail, we extracted from the periodic DFTB-MD studies the reaction pathways and carried out the finite cluster QM calculation using the B3LYP functional with the 6-311++G(d,p) basis set as implemented in Jaguar.[34] This choice best reproduces the high quality CCSD(T)/6-311++G(d,p) results for two smaller N-rich model compounds, tetrazole and 1-hydroxy-5-H-tetrazole, but with much less computational cost, as shown in Tables S2 and S3, Figures S1 and S2 of SI. To model the electrostatic interaction between the explicit molecules in the finite QM with the polar environment that the negatively charged TKX-50 sees due to the hydroxylammonium cations in the crystal, we applied the Poisson−Boltzmann solvation model[35] (implicit solvent) using a dielectric constant of 77.74 and a spherical cavity of radius 2.21 Å for NH_2OH, the conjugate base of hydroxylammonium. The transition states were validated to have exactly one negative eigenvalue of the Hessian. We then followed the minimum energy path to identify and connect to reactant and product. Thermodynamic properties were evaluated at 298.15 K and 1 atm. All barriers reported in this paper, if not specified, are enthalpic barriers.

3. RESULTS AND DISCUSSION

3.1. Reaction Mechanisms at High Temperatures from DFTB-MD Simulations. To examine the chemical reactions in TKX-50, we analyzed the molecular fragments during the cook-off simulation, which are plotted in Figure 2 as a function of temperature. The starting supercell contains 16 hydroxylammonium $(NH_3OH)^+$ and 8 diolate $(C_2O_2N_8)^{2-}$ as shown in Figure 2a. As the temperature increases to 491 K (1.05 ps) and a pressure of 0.01 GPa, we observe proton transfer reactions, leading to formation of the conjugate base hydroxylamine

dx.doi.org/10.1021/jp509582x | J. Phys. Chem. C 2014, 118, 27175−27181

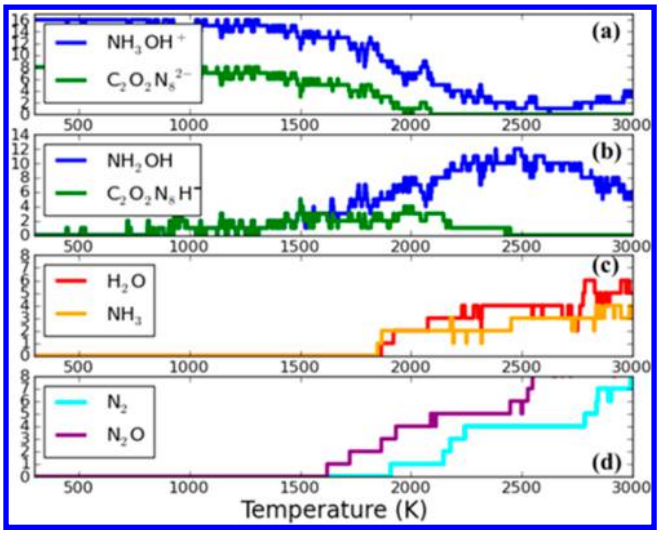

Figure 2. Fragment analyses during the cook-off simulation of TKX-50 as the temperature is ramped at a uniform rate of 180 K/ps from 300 to 3000 K. (a) the reactants: hydroxylammonium $(NH_3OH)^+$ and diolate $(C_2O_2N_8)^{2-}$. (b) The conjugate acid and base hydroxylamine (NH_2OH) and H-diolate $(H\text{-}C_2O_2N_8)^-$ that are produced by proton transfer reactions. (c) Two stable species (H_2O and NH_3) that are the products of the decomposition and recombination of $(NH_3OH)^+$. (d) Two stable species (N_2 and N_2O), indicating ring breaking reactions in H-diolate.

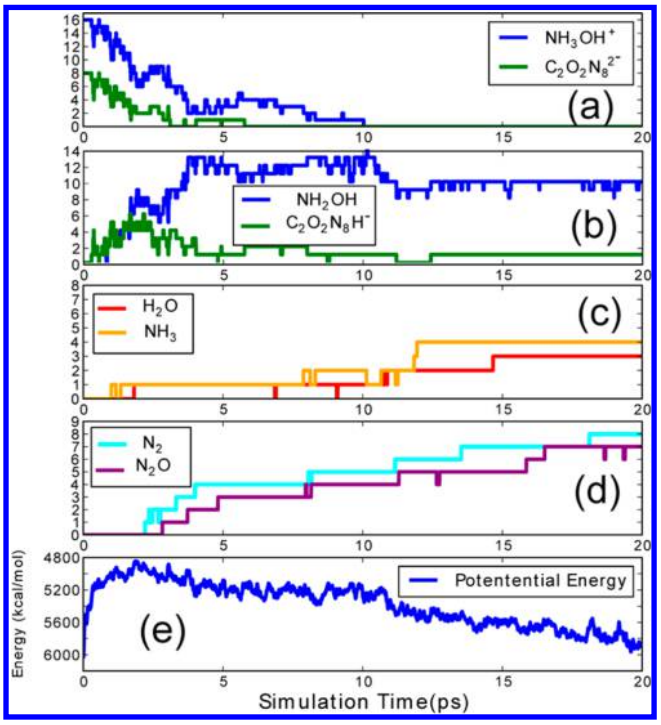

Figure 3. Fragment analysis over the 20 ps DFTB-MD simulation of TKX-50 at 1750 K. (a) the reactants: hydroxylammonium $(NH_3OH)^+$ and diolate $(C_2O_2N_8)^{2-}$. (b) Conjugate acid and base hydroxylamine (NH_2OH) and H-diolate $(H\text{-}C_2O_2N_8)^-$ that are the products of the proton transfer reaction. (c) Two stable species H_2O and NH_3 from decomposition of the hydroxylamine. (d) Two stable species N_2 and N_2O, from decomposition of the diolate ring. (e) Potential energy during the simulation (in the unit of kcal/mol), showing a maximum at the point of the N_2 release.

Table 1. Reactions of N_2 and N_2O Releasing Observed during 20 ps NVT and the Corresponding Number of Occurrences

	reactions	number of occurrences
N_2 formation	$HO_2C_2N_8 = HO_2C_2N_6 + N_2$	3
	$H_2O_2C_2N_8 = H_2O_2C_2N_6 + N_2$	2
N_2O formation	$HO_2C_2N_8 = HOC_2N_6 + N_2O$	1
	$OC_2N_5 = N_2O + C_2N_3$	1
	$HOC_2N_6 = N_2O + HC_2N_4$	1
	$HO_2C_2N_6 = N_2O + HOC_2N_4$	1
	$H_2O_2C_2N_6 = H_2OC_2N_4 + N_2O$	1

(NH_2OH) and acid H-diolate $(H\text{-}C_2O_2N_8)^-$, as shown in Figure 2b. Below 1500 K the H-diolate does not react, indicating that proton transfer from $(NH_3OH)^{1+}$ to $(C_2O_2N_8)^{2-}$ is the only chemical reaction. Finally at around 1700 K and 1.06 GPa, N_2O appears and at 1900 K and 1.68 GPa, N_2 appears, as shown in Figure 2d. These products indicate that the $(C(NO)N_3)$ ring has broken. We consider these ring breaking reactions as the most important in the initial reactions of TKX-50 because they lead to energy release to provide the starting point of subsequent decomposition reactions. As the temperature continues increasing above 1900 K with a pressure of 1.68 GPa, we observe the secondary products H_2O and NH_3 as shown in Figure 2c, indicating the decomposition and recombination of hydroxylammonium $(NH_3OH)^+$.

Figure 3 shows the fragment analysis during 20 ps NVT simulation at 1750 K along with the potential energy curve. The initial reaction (starting at 0.2 ps and pressure of 0.01 GPa) is still the proton transfer. Then H_2O and NH_3 appear from the decomposition of the neutralized cations (NH_2OH). This reaction occurs earlier than the ring breaking process (in the cook-off simulation, it happened after ring breaking). At about 2.5 ps and a pressure of 1.39 GPa, N_2 appears, indicating that a ring has broken. At this point the potential energy begins to decrease, since N_2 release is exothermic. This is important because this energy release may induce other reactions. Most of the N_2O comes from further decomposition of the ring after releasing N_2. The other fragments appearing in this simulation are shown in Figure S3 of SI.

The main reactions are summarized in Table 1. We observed that one or two protons always attaches to the ring before its decomposition. This indicates that proton transfer catalyzes the ring breaking reactions. It is especially interesting that N_2 appears earlier than N_2O in the fixed temperature simulation, in contrast to our cook-off simulations. On the basis of transition state theory, the reaction rate depends on the activation energy, the temperature, and the pre-exponential factor. The cook-off simulation with its extremely fast heating rate may lead to modified kinetics, so we consider fixed temperature simulation to be more reliable in deducing the initial reactions. For fixed temperature simulations, N_2 release occurred first, indicating an activation energy barrier lower than for N_2O release. We will examine these reaction barriers in the next section to determine the correct reaction sequence in the ring breaking processes.

3.2. Reaction Mechanism from Finite Cluster QM Calculation. For many ionic solids, the barrier for proton transfer is less than 10 kcal/mol,[36] much lower than for the normal initial reaction in the EMs, >35 kcal/mol. This is

dx.doi.org/10.1021/jp509582x | J. Phys. Chem. C 2014, 118, 27175−27181

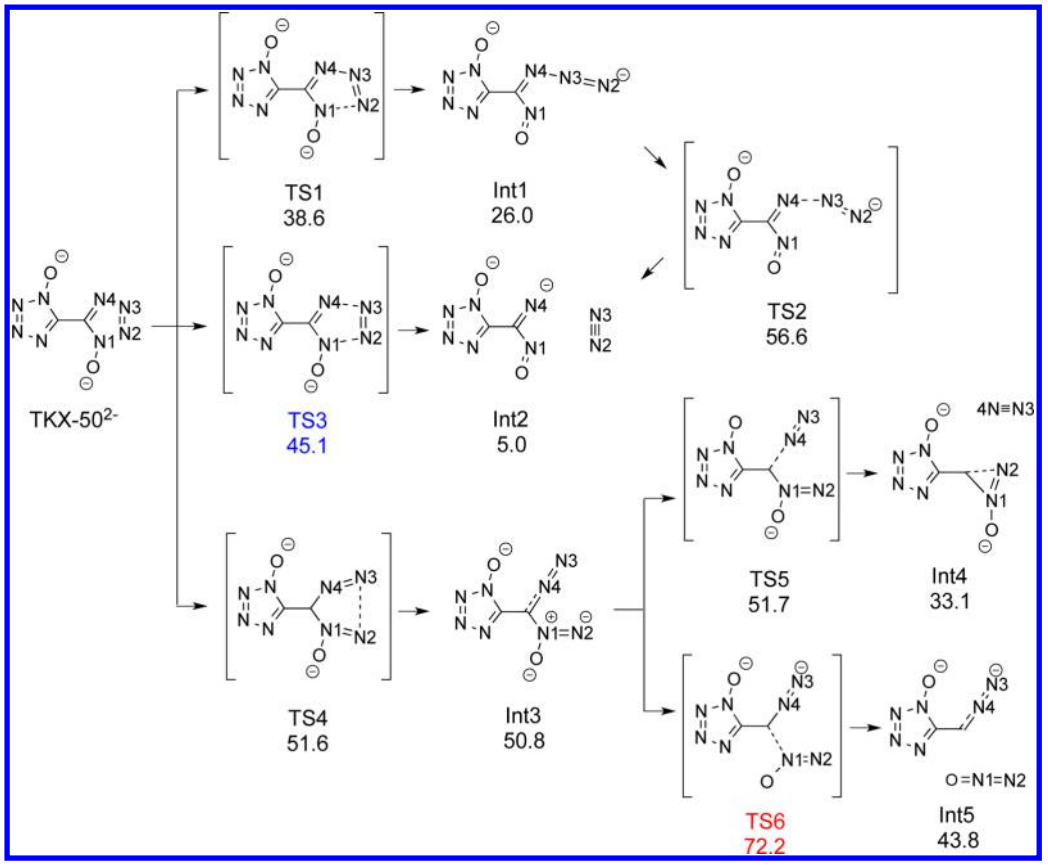

Figure 4. Unimolecular decomposition reactions and corresponding enthalpies (kcal/mol) for TKX-50 dianion from finite QM (B3LYP). The rate-determining steps to give N_2 and N_2O production are indicated in blue (TS3, 45.1 kcal/mol) and red (TS6, 72.2 kcal/mol), respectively. We conclude that for the dianion, the most favorable N_2 release path has a barrier of 45.1 kcal/mol with a reaction energy of 5.0 kcal/mol, while the most favorable N_2O release path has a barrier of 72.2 kcal/mol with a reaction energy of 43.8 kcal/mol.

consistent with our DFTB-MD simulations where we observed that the proton transfer happens very early (491 K).

We now focus on the ring breaking reactions of the TKX-50 dianion $(O_2C_2N_8)^{2-}$ and four prototropic tautomers $(H-O_2C_2N_8)^{1-}$ after the proton has already transferred from the hydroxylammonium to one of the four different basic sites of TKX-50 dianion.

Starting with dianionic TKX-50 shown in Figure 4, the easiest reaction path to open the five-member ring is to break the N1−N2 bond via TS1 to form an azide intermediate Int1, which we find to have a barrier of 38.6 kcal/mol. However, the decomposition of this azide intermediate has a high barrier (56.6 kcal/mol) to produce N_2. Instead N_2 production can be obtained via a concerted reaction (TS3) with only 45.1 kcal/mol barrier, rendering it the easiest path to break the five-member ring of TKX-50.

To generate N_2O, the five-member ring first breaks the N2−N3 bond via TS4 (51.6 kcal/mol) to give a diazo intermediate Int3 from which the N_2O dissociates via TS6 with a considerable barrier (72.2 kcal/mol). It is also possible to dissociate N_2 from Int3. However, the barrier (51.7 kcal/mol) is higher than the reaction path via TS3 with only 45.1 kcal/mol barrier.

To examine how proton transfer affects the decomposition of TKX-50, we placed a proton on the four different basic sites of the five-member ring, leading to four prototropic tautomers: Int6, Int10, Int13 and Int17, as shown in Figure 5. The easiest fragmentation pathway to give N_2 starts with Int10, where the proton is transferred to O, followed by a step in which two N−N bonds break simultaneously (TS12, 37.2 kcal/mol) to Int12. The other concerted reaction pathway starting from Int13 via TS16 to Int16 also has a similar barrier height of 39.2 kcal/mol, but with much higher exothermicity of 14.7 kcal/mol. Since the N_2 release reaction occurs after proton has transferred, this reaction could be considered as a two-step reaction. Thus, the reaction barriers are 29.8 kcal/mol through TS12 to Int12 and 35.0 kcal/mol through TS16 to Int16 where we reference to the one-proton-attached structures. These two pathways have barrier heights 6−8 kcal/mol lower than the case of dianionic TKX-50, indicating that proton transfer reaction facilitates the decomposition of TKX-50.

For the N_2O product, the easiest fragmentation pathway starts with Int13, followed by a concerted two N−N bond-breaking step (TS13, 59.5 kcal/mol) to Int14. Compared with the dianionic TKX-50, the barrier height is 12.7 kcal/mol lower if assisted by the proton transfer. Note that all proton transfer events from hydroxylammonium to TKX-50 dianion are enthalpically uphill, which increases the barrier for reactions via TS9 and TS14 compared with TS1. This indicates that not all reactions are assisted by proton transfer. However, the reaction pathways responsible for N_2 and N_2O production have lower barriers in the monanionic case even with the extra enthalpic cost to transfer the proton. This supports our results from DFTB-MD that proton transfer catalyzes decomposition of the N-rich ring.

The initial reaction of TKX-50 involves ring breaking to release N_2 rather than release of N_2O because breaking the CN bond is necessary for N_2O release, while releasing N_2 requires

dx.doi.org/10.1021/jp509582x | J. Phys. Chem. C 2014, 118, 27175−27181

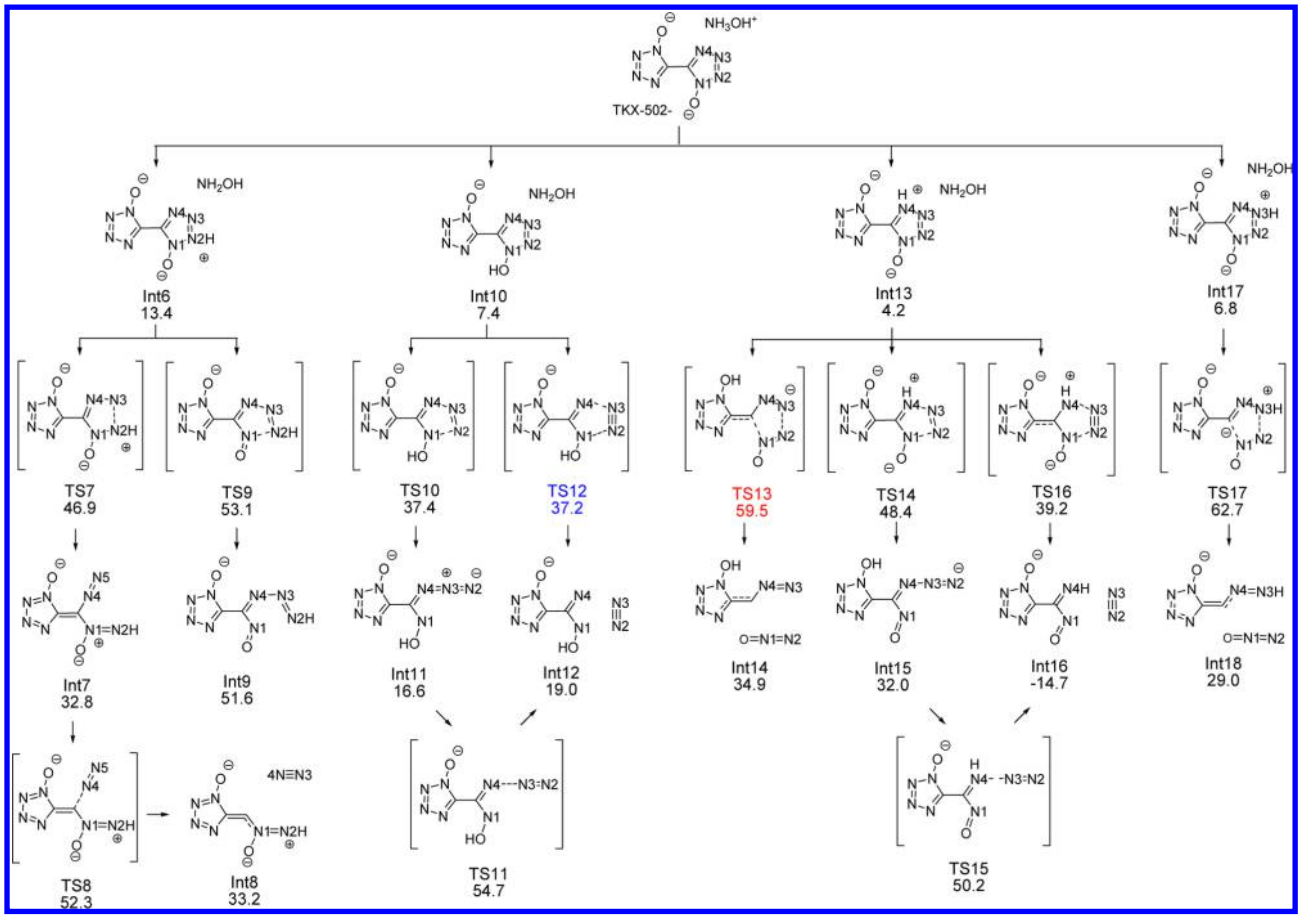

Figure 5. Decomposition reactions and corresponding enthalpies (kcal/mol) of TKX-50 prototropic tautomers. The rate-determining steps to produce N_2 and N_2O are in blue (TS12 at 37.2 kcal/mol) and red (TS13 at 59.5 kcal/mol), respectively. We conclude that for the protonated monanion, the most favorable N_2 release path has a barrier of 37.2 kcal/mol and a reaction energy of 19.0 kcal/mol after proton transfer, while the most favorable N_2O release path has a barrier of 59.5 kcal/mol and a reaction energy of 34.9 kcal/mol.

only breaking the weaker NN bond. Also the N_2 release reaction through TS16 to Int16 is exothermic, whereas N_2O release reactions are endothermic, leading to accelerating subsequent release of N_2 from other TKX-50 molecules.

In DFTB-MD simulations, we also observed the N_2 releasing reaction after two protons attached to two N4 sites of the double ring. The calculated decomposition reaction pathway is shown in Figure 6. Using the same reference state, we find a reaction barrier is 51.5 kcal/mol with an release energy of 5.2 kcal/mol. However, taking $H_2O_2C_2N_8$ as the reference structure, the reaction barrier is decreased to 36.3 kcal/mol, which is very similar to the N_2 release reaction through TS16 (35.0 kcal/mol) to Int16 for the one proton case. This indicates that adding the second proton to the ring does not change the rate of N_2 release.

Developing the azole-based, nitrogen-rich heterocycles compounds is essential for the next generation explosives because they are highly endothermic with high densities and low sensitivities toward outer stimuli and are easily synthesized with little environmental impact. TKX-50 is one of these promising compounds. Our finding that the proton transfer reaction precedes the reactions of the bistetrazole, with its effects on decreasing the reaction barriers for breaking ring might also be important in other similar explosives.

4. CONCLUSIONS

Summarizing, we examined the initial chemical reactions of the newly synthesized explosive TKX-50 by combining DFTB-MD periodic simulations to discover the feasibility of proton transfer with a low barrier with finite cluster quantum calculations to obtain more accurate barriers. Key points from the simulations are

- The proton transfer happens at a much low temperature than the ring breaking reaction.
- The initial reaction involves ring breaking to release N_2 rather than ring breaking to release N_2O.
- The proton transfer decreases the reaction barrier for both releases of N_2 and N_2O by ~10 kcal/mol.

These simulations suggest that the strategy to design less sensitive azole-based HEDMs is to prevent the proton transfer between the cation and anion. This can be achieved replacing the cation with a stronger base, for example, NH_4^+, $N_2H_5^+$, and $H(CH_2)_2NH_3^+$. On the basis of their pK_a values of 9.24, 7.99, and 10.64 relative to 5.98 for $(NH_3OH)^+$,[37] we estimate that the temperature for proton transfer in our simulations might have increased to 511, 504, and 518 K, respectively, compared to 491 K for $(NH_3OH)^+$. Of course, the sensitivity of explosives is also related to other factors such as steric hindrance, defects, solvent entrainment, and grain boundaries that must also be examined for new explosives.

dx.doi.org/10.1021/jp509582x | J. Phys. Chem. C 2014, 118, 27175−27181

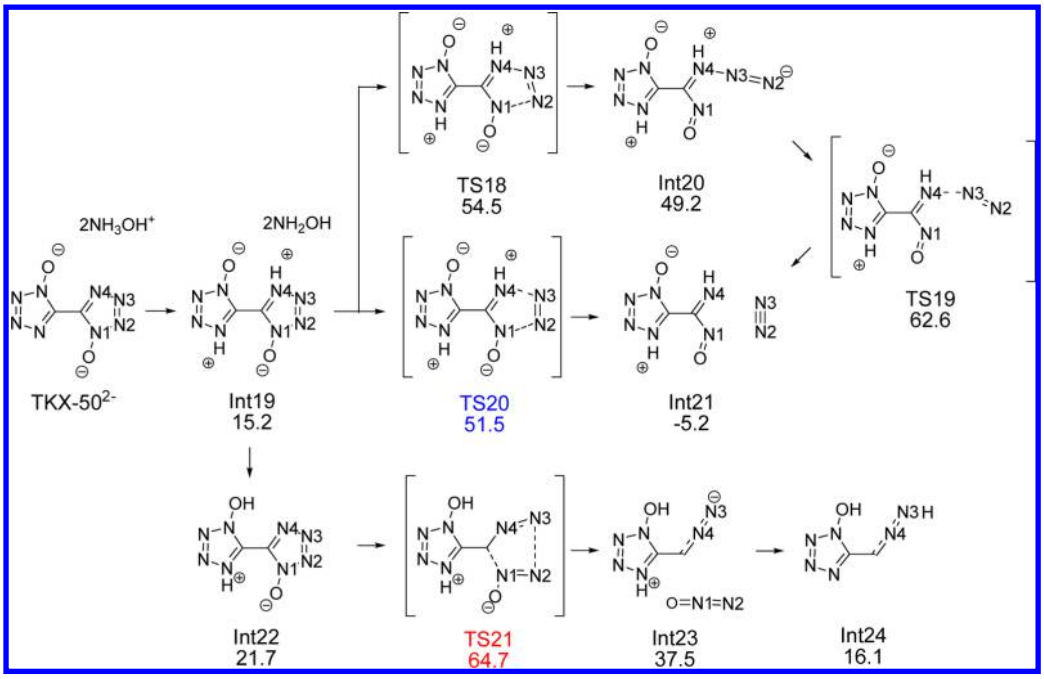

Figure 6. Decomposition reactions and corresponding enthalpies (kcal/mol) of TKX-50 for the protonated neutral system observed in the DFTB-MD NVT simulations. Relative to the dianion starting point, the N_2 release path has a barrier of 51.5 kcal/mol and release energy of 5.2 kcal/mol. However, relative to the Int19 protonated intermediate, the barrier is 36.3 kcal/mol, similar to the barrier of 37.2 for TS12 (Figure 5), indicating that protonating the other ring had little effect on the N_2 release.

■ ASSOCIATED CONTENT

Supporting Information

Tables of bond type and bond cutoff for the fragment analysis, the electronic energies of decomposition reactions species for tetrazole and 1-hydroxy-5-H-tetrazole using various *ab initial* methods. It also includes figures showing decomposition reaction mechanisms of tetrazole and 1-hydroxy-5-H-tetrazole, and the fragments observed during the NVT simulations at 1750 K besides those in Figure 3. This material is available free of charge via the Internet at http://pubs.acs.org.

■ AUTHOR INFORMATION

Corresponding Author

*E-mail: wag@wag.caltech.edu.

Author Contributions

‡Q.A. and W.-G.L. contributed equally to this paper.

Notes

The authors declare no competing financial interest.

■ ACKNOWLEDGMENTS

We thank Dr. Cliff Bedford, Dr. Al Stern, and Prof. Tom Klapötke for suggesting the study of TKX-50. This research was funded by ONR (N00014-09-1-0634, Cliff Bedford).

■ REFERENCES

(1) Badgujar, D. M.; Talawar, M. B.; Asthana, S. N.; Mahulikar, P. P. Advances in Science and Technology of Modern Energetic Materials: An Overview. *J. Hazard. Mater.* **2008**, *151*, 289−305.

(2) Klapötke, T. *Chemistry of High-Energy Materials*, 2nd ed.; de Gruyter: Berlin, 2012.

(3) Sikder, A. K.; Sikder, N. A Review of Advanced High Performance, Insensitive and Thermally Stable Energetic Materials Emerging for Military and Space Applications. *J. Hazard. Mater.* **2004**, *112*, 1−15.

(4) Bolton, O.; Matzger, A. J. Improved Stability and Smart-Material Functionality Realized in an Energetic Cocrystal. *Angew. Chem., Int. Ed.* **2011**, *50*, 8960−8963.

(5) Talawar, M. B.; Sivabalan, R.; Mukundan, T.; Muthurajan, H.; Sikder, A. K.; Gandhe, B. R.; Rao, A. S. Environmentally Compatible Next Generation Green Energetic Materials (GEMs). *J. Hazard. Mater.* **2009**, *161*, 589−607.

(6) Dippold, A. A.; Klapötke, T. A Study of Dinitro-bis-1,2,4-triazole-1,1′-diol and Derivatives: Design of High-Performance Insensitive Energetic Materials by the Introduction of N-Oxides. *J. Am. Chem. Soc.* **2013**, *135*, 9931−9938.

(7) An, Q.; Xiao, H.; Goddard, W. A., III; Meng, X. Y. Stability of NNO and NPO Nanotube Crystals. *J. Phys. Chem. Lett.* **2014**, *5*, 485−489.

(8) Fisher, N.; Fisher, D.; Klapötke, T.; Piercey, D. G.; Stierstorfer, J. Pushing the Limits of Energetic Materials − the Synthesis and Characterization of Dihydroxylammonium 5,5′-bistetrazole-1,1′-Diolate. *J. Mater. Chem.* **2012**, *22*, 20418−20422.

(9) Brill, T. B.; James, K. J. Kinetics and Mechanisms of Thermal Decomposition of Nitroaromatic Explosives. *Chem. Rev.* **1993**, *93*, 2667−2692.

(10) Brill, T. B.; Gongwer, P. E.; Williams, G. K. Thermal Decomposition of Energetic Materials. 66. Kinetic Compensation Effects in HMX, RDX, and NTO. *J. Phys. Chem.* **1994**, *98*, 12242−12247.

(11) Behrens, R., Jr.; Bulusu, S. Thermal Decomposition of Energetic Materials. 3. Temporal Behaviors of the Rates of Formation of the Gaseous Pyrolysis Products from Condensed-Phase Decomposition of 1,3,5-Trinitrohexahydro-s-triazine. *J. Phys. Chem.* **1992**, *96*, 8877−8891.

(12) Maharrey, S.; Behrens, R., Jr. Thermal Decomposition of Energetic Materials. 5. Reaction Processes of 1,3,5-Trinitrohexahydro-s-triazine below Its Melting Point. *J. Phys. Chem. A* **2005**, *109*, 11236−11249.

(13) Manna, M. R.; Fried, L. E.; Reed, E. J. Explosive Chemistry: Simulating the Chemistry of Energetic Materials at Extreme Conditions. *J. Comput.-Aided Mater. Des.* **2003**, *10*, 75−97.

(14) Sharia, O.; Kuklja, M. M. Rapid Materials Degradation Induced by Surfaces and Voids: Ab Initio Modeling of β-Octatetramethylene Tetranitramine. *J. Am. Chem. Soc.* **2012**, *134*, 11815−11820.
(15) Chakraborty, D.; Muller, R. P.; Dasgupta, S.; Goddard, W. A., III The Mechanism for Unimolecular Decomposition of RDX (1,3,5-Trinitro-1,3,5-triazine), an *ab Initio* Study. *J. Phys. Chem. A* **2000**, *104*, 2261−2272.
(16) Chakraborty, D.; Muller, R. P.; Dasgupta, S.; Goddard, W. A., III Mechanism for Unimolecular Decomposition of HMX (1,3,5,7-Tetranitro-1,3,5,7-tetrazocine), an *ab Initio* Study. *J. Phys. Chem. A* **2001**, *105*, 1302−1314.
(17) Furman, D.; Kosloff, R.; Dubnikova, F.; Zybin, S. V.; Goddard, W. A., III; Rom, N.; Hirshberg, B.; Zeiri, Y. Decomposition of Condensed Phase Energetic Materials: Interplay between Uni- and Bimolecular Mechanisms. *J. Am. Chem. Soc.* **2014**, *136*, 4192−4200.
(18) Minier, L. M.; Brower, K. R.; Oxley, J. C. Role of Intermolecular Reactions in Thermolysis of Aromatic Nitro Compounds in Supercritical Aromatic Solvents. *J. Org. Chem.* **1991**, *56*, 3306−3314.
(19) Liu, W. G.; Zybin, S. V.; Dasgupta, S.; Klapötke, T. M.; Goddard, W. A., III Explanation of the Colossal Detonation Sensitivity of Silicon Pentaerythritol Tetranitrate (Si-PETN) Explosive. *J. Am. Chem. Soc.* **2009**, *131*, 7490−7491.
(20) An, Q.; Goddard, W. A., III; Zybin, S. V.; Jaramillo-Botero, A.; Zhou, T. T. Highly Shocked Polymer Bonded Explosives at a Nonplanar Interface: Hot-Spot Formation Leading to Detonation. *J. Phys. Chem. C* **2013**, *117*, 26551−26561.
(21) Rahm, M.; Brink, T. Kinetic Stability and Propellant Performance of Green Energetic Materials. *Chem.—Eur. J.* **2010**, *16*, 6590−6600.
(22) Gruzdkov, Y. A.; Dreger, Z. A.; Gupta, Y. M. Experimental and Theoretical Study of Pentaerythritol Tetranitrate Conformers. *J. Phys. Chem. A* **2004**, *108*, 6216−6221.
(23) Dreger, Z. A.; Gupta, Y. M. High Pressure−High Temperature Polymorphism and Decomposition of Pentaerythritol Tetranitrate (PETN). *J. Phys. Chem. A* **2013**, *117*, 5306−5313.
(24) Tas, G.; Franken, J.; Hambir, S. A.; Hare, D. E.; Dlott, D. D. Ultrafast Raman Spectroscopy of Shock Fronts in Molecular Solids. *Phys. Rev. Lett.* **1997**, *78*, 4585−4588.
(25) Franken, J.; Hambir, S. A.; Dlott, D. D. Ultrafast Shock-induced Orientation of Polycrystalline Films: Applications to High Explosives. *J. Appl. Phys.* **1999**, *85*, 2068−2074.
(26) Zhou, L.; Piekiel, N.; Chowdhury, S.; Zachariah, M. R. T-Jump/time-of-flight Mass Spectrometry for Time-Resolved Analysis of Energetic Materials. *Rapid Commun. Mass Spectrom.* **2009**, *23*, 194−202.
(27) Elstner, M.; Porezag, D.; Jungnickel, G.; Elsner, J.; Haugk, M.; Frauenheim, Th.; Suhai, S.; Seifert, G. Self-Consistent-Charge Density-Functional Tight-Binding Method for Simulations of Complex Materials Properties. *Phys. Rev. B* **1998**, *58*, 7260−7268.
(28) Manaa, M. R.; Fried, L. E.; Reed, E. J. Explosive Chemistry: Simulating the Chemistry of Energetic Materials at Extreme Conditions. *J. Comput.-Aided Mater. Des.* **2003**, *10*, 75−97.
(29) Margetis, D.; Kaxiras, E.; Elstner, M.; Frauenheim, T.; Manaa, M. R. Electronic Structure of Solid Nitromethane: Effects of High Pressure and Molecular Vacancies. *J. Chem. Phys.* **2002**, *117*, 788−799.
(30) Reed, E. J.; Rodriguez, A. W.; Manaa, M. R.; Fried, L. E.; Tarver, C. M. Ultrafast Detonation of Hydrazoic Acid (HN3). *Phys. Rev. Lett.* **2012**, *109*, 038301.
(31) Aradi, B.; Hourahine, B.; Frauenheim, T. DFTB+, a Sparse Matrix-Based Implementation of the DFTB Method. *J. of Phys. Chem. A* **2007**, *111*, 5678−5684.
(32) Gaus, M.; Goez, A.; Elstner, M. Parametrization and Benchmark of DFTB3 for Organic Molecules. *J. Chem. Theory Comput.* **2013**, *9*, 338−354.
(33) Rappe, A. K.; Casewit, C. J.; Colwell, K. S.; Goddard, W. A., III; Skiff, W. M. UFF, a Full Periodic Table Force Field for Molecular Mechanics and Molecular Dynamics Simulations. *J. Am. Chem. Soc.* **1992**, *114*, 10024−10035.
(34) Bochevarov, A. D.; Harder, E.; Hughes, T. F.; Greenwood, J. R.; Braden, D. A.; Philipp, D. M.; Rinaldo, D.; Halls, M. D.; Zhang, J.; Friesner, R. A. Jaguar: A High-Performance Quantum Chemistry Software Program with Strengths in Life and Materials Sciences. *Int. J. Quantum Chem.* **2013**, *113*, 2110−2142.
(35) Perry, D. L.; Phillips, S. L. *Handbook of Inorganic Compounds*; Taylor & Francis: New York, 1995.
(36) Colomban, P. *Proton Conductors: Solids, Membranes and Gels - Materials and Devices*; Cambridge University Press: Cambridge, UK, 1992.
(37) Williams, R. *pKa Data*. Available from http://www.research.che.edu.psu.edu/brpgroup/pKa_compilation.pdf.